PENNSTATE

Applied Research Laboratory

FOURTH MOMENTS OF ACOUSTIC WAVES FORWARD SCATTERED BY A ROUGH OCEAN SURFACE

C.C. YANG and S.T. MCDANIEL

Technical Memorandum
File No. 90-227
SE90-67
9 August 1990

Copy No. 18

Unlimited Distribution

Applied Research Laboratory
P.O. Box 30
State College, PA 16804
(814) 865-3031

PENNSTATE

Applied Research Laboratory

FOURTH MOMENTS OF ACOUSTIC WAVES FORWARD SCATTERED BY A ROUGH OCEAN SURFACE

C.C. YANG and S.T. MCDANIEL

Technical Memorandum
File No. 90-227
SE90-67
9 August 1990

Copy No. 18

Unlimited Distribution

Applied Research Laboratory
P.O. Box 30
State College, PA 16804
(814) 865-3031

REPORT DOCUMENTATION PAGE

Form Approved
OMB No. 0704-0188

1. AGENCY USE ONLY (Leave blank)	2. REPORT DATE	3. REPORT TYPE AND DATES COVERED
	9 August 1990	Final Technical Report 2/15/89-2/14/90

4. TITLE AND SUBTITLE
Fourth Moments of Acoustic Waves Forward Scattered by a Rough Ocean Surface

5. FUNDING NUMBERS
N00014-89-J-1690

6. AUTHOR(S)
C. C. Yang and S. T. McDaniel

7. PERFORMING ORGANIZATION NAME(S) AND ADDRESS(ES)
Applied Research Laboratory
The Pennsylvania State University
P. O. Box 30
State College, PA 16804

8. PERFORMING ORGANIZATION REPORT NUMBER
ARL TM 90-227

9. SPONSORING/MONITORING AGENCY NAME(S) AND ADDRESS(ES)
Office of Naval Research
800 North Quincy Street
Arlington, VA 22217-5000

10. SPONSORING/MONITORING AGENCY REPORT NUMBER

11. SUPPLEMENTARY NOTES

12a. DISTRIBUTION/AVAILABILITY STATEMENT
Unlimited

12b. DISTRIBUTION CODE

13. ABSTRACT *(Maximum 200 words)*

Three types of statistical fourth moments of acoustic waves forward scattered by a randomly rough ocean surface are derived and numerically evaluated. The first one is related to the scintillation index which characterizes intensity fluctuations. The second one is the two-position intensity correlation function which describes the spatial correlation of wave intensity. The third is the two-position coherence function which carries information on the phase fluctuations of the scattered wave. In the range of weak scattering, the ratio of the absolute value of the two-position coherence function over the two-position intensity correlation exactly describes the mean square fluctuation of the relative phase between the two positions. The acoustic frequency is high so that the Kirchhoff approximation can be used. Two types of spectral functions for surface-height fluctuations are considered: a Gaussian spectrum and the Donelan/Pierson spectrum. The latter is obtained from a model for the fluctuations of the ocean surface height which are controlled by the wind speed at the ocean surface.

14. SUBJECT TERMS
Forward scattering, ocean surface, high frequency scattering statistics

15. NUMBER OF PAGES
40

16. PRICE CODE

17. SECURITY CLASSIFICATION OF REPORT	18. SECURITY CLASSIFICATION OF THIS PAGE	19. SECURITY CLASSIFICATION OF ABSTRACT	20. LIMITATION OF ABSTRACT
Unclassified	Unclassified	Unclassified	Unlimited

From: C. C. Yang and S. T. McDaniel

Subject: Fourth Moments of Acoustic Waves Forward Scattered by a Rough Ocean Surface

References: See pages 24 and 25

Abstract:

Three types of statistical fourth moments of acoustic waves forward scattered by a randomly rough ocean surface are derived and numerically evaluated. The first one is related to the scintillation index which characterizes intensity fluctuations. The second one is the two-position intensity correlation function which describes the spatial correlation of wave intensity. The third is the two-position coherence function which carries information on the phase fluctuations of the scattered wave. In the range of weak scattering, the ratio of the absolute value of the two-position coherence function over the two-position intensity correlation exactly describes the mean square fluctuation of the relative phase between the two positions. The acoustic frequency is high so that the Kirchhoff approximation can be used. Two types of spectral functions for surface-height fluctuations are considered: a Gaussian spectrum and the Donelan/Pierson spectrum. The latter is obtained from a model for the fluctuations of the ocean surface height which are controlled by the wind speed at the ocean surface.

TABLE OF CONTENTS

LIST OF FIGURES

Page

I. INTRODUCTION

Although the study of wave scattering by randomly rough surfaces started several decades ago, it is still a challenging research topic today [1-11]. Basically, when the surface is slightly rough and its surface slope is generally smaller than unity, the perturbation technique can be used. When the radius of curvature of the surface is much greater than the wavelength, the Kirchhoff approximation can be applied [12]. In other words, for relatively long wavelength waves, the perturbation technique is a good choice; for relative short wavelength waves, the Kirchhoff approximation can be adopted. In any situation, second moments of the scattered wave field can provide some useful information such as average intensity. More fruitful information on scattering characteristics relies upon the knowledge of fourth moments of the scattered wave field. However, more difficulties will be encountered in deriving the fourth moments. Wave scattering by randomly rough surfaces is not only an interesting topic for theoretical study but also a practical problem in many applications ranging from microwave scattering by ground surfaces in remote sensing, acoustic scattering by the ocean surface and floor in underwater acoustics, to optical scattering by a rough metal, dielectrics, or semiconductor surfaces in designing optics and electronics devices.

In this paper, three types of fourth moments are evaluated for acoustic waves forward scattered by a rough ocean surface. The first one is the scintillation index σ defined by

$$\sigma = [\langle |p|^4 \rangle / \langle |p|^2 \rangle^2 - 1]^{1/2} . \tag{1}$$

Here p is the scattered acoustic wave field and < > stands for an ensemble average. The scintillation index describes the intensity fluctuation of the scattered wave. The purpose of evaluating the other two fourth moments is to extract some information on the phase fluctuation of the scattered wave. To see this point, let us first consider the case of weak scattering in which the fluctuations of the log-amplitude and phase of the scattered wave field are either weak or jointly Gaussian distributed. Hence, by writing the scattered wave p as

$$p = \exp(\chi + iS) \tag{2}$$

in terms of the log-amplitude χ and phase S, the two-position coherence function $\langle (p_1 p_2^*)^2 \rangle$ is given by

$$\begin{aligned} \langle (p_1 p_2^*)^2 \rangle &= \exp[2\langle (\chi_1 + \chi_2)^2 \rangle] \exp[-2\langle (S_1 - S_2)^2 \rangle] \\ &\times \exp[4i\langle (\chi_1 + \chi_2)(S_1 - S_2) \rangle] \quad , \end{aligned} \tag{3}$$

where the subscripts 1 and 2 stand for the waves at positions 1 and 2, respectively. Meanwhile, the two-position intensity correlation function $\langle I_1 I_2 \rangle$ is given by

$$\begin{aligned} \langle I_1 I_2 \rangle &= \langle |p_1|^2 |p_2|^2 \rangle \\ &= \exp[2\langle (\chi_1 + \chi_2)^2 \rangle] \end{aligned} \tag{4}$$

where the intensity $I = |p|^2$. Therefore,

$$\frac{|\langle (p_1 p_2^*)^2 \rangle|}{\langle I_1 I_2 \rangle} = \exp[-2\langle (S_1 - S_2)^2 \rangle] \tag{5}$$

which describes the fluctuation of the relative phase between the two observation positions. When scattering becomes stronger, the simple result in Eq. (5) is not

valid. However, the ratio $|\langle(p_1p_2^*\rangle|/\langle I_1I_2\rangle$ or the difference between $|\langle(p_1p_2^*)^2|$ and $\langle I_1I_2\rangle$ still carries information on the relative phase fluctuations. To extract this information, the normalized two-position coherence function $\langle(p_1p_2^*)^2/\langle I_1\rangle\langle I_2\rangle$ and normalized two-position intensity correlation function $\langle I_1I_2\rangle/\langle I_1\rangle\ \langle I_2\rangle$ are to be evaluated in this paper.

Because the acoustic frequency of concern is relatively high, the Kirchhoff approximation will be used. Two types of spectral functions for the surface-height fluctuation are considered: a Gaussian spectrum and the Donelan/Pierson (D/P) spectrum. The latter is obtained from a model describing the fluctuations of the ocean surface height which are controlled by the wind speed on the ocean surface [13]. Both the scale-size and mean-square fluctuation of the ocean surface height are determined by the wind speed. The fluctuation of surface height ζ is assumed to be statistically Gaussian distribu ed. Numerical techniques will be designed to evaluate the multi-fold integrations of the fourth moments. For mathematical simplicity, only two-dimensional propagation and scattering are considered. The rest of this paper is organized as follows. The geometry of problem is discussed in section II. Also, the average intensity of the scattered wave field is evaluated. The derivations and numerical results for the scintillation index are given in section III. Sections IV and V are devoted to evaluation of the two-position coherence function and two-position correlation function, respectively. Conclusions are drawn in section VI.

II. GEOMETRY OF PROBLEM

The basic geometry of two-dimensional scattering by a randomly scattered rough ocean surface is shown in Figure 1a. The depth and smooth ocean surface are defined to be along the z and x axes, respectively. A line source and a line

receiver are located at certain depths so that the incident range R_i, scattering range R_s, incident angle θ_i, and scattering angle θ_s, are as shown in the figure. The surface height fluctuation from the mean at z = 0 is described by the random field $\zeta(x)$ with $\langle\zeta(x)\rangle = 0$. By ignoring some unimportant factors, the wave field at the receiver in the Kirchhoff approximation can be expressed by [14]

$$p = \int_{-\infty}^{\infty} dx \exp\left[-i\left(x^2/x_f^2 + 2\alpha x + 2\gamma\zeta(x)\right)\right] \tag{6}$$

where

$$x_f^2 = \frac{2}{k}\left(\frac{\sin^2\theta_i}{R_i} + \frac{\sin^2\theta_s}{R_s}\right)^{-1} \tag{7}$$

$$\alpha = \frac{k}{2}(\cos\theta_i - \cos\theta_s) \tag{8}$$

and

$$\gamma = -\frac{k}{2}(\sin\theta_i + \sin\theta_s) \quad . \tag{9}$$

Here k is the wave number which is assumed to be a constant in the ocean. In other words, the ocean is assumed to be a homogeneous medium to the sound wave. In Eq. (6), since $\zeta(x)$ is a random field, the wave field p is stochastic. Note that the coordinate center can be properly chosen so that $\theta_i = \theta_s = \theta$ and, hence, $\alpha = 0$.

The average intensity of the scattered wave field can be easily computed to give

$$\langle I\rangle = \langle|p|^2\rangle = \pi x_f^2 \tag{10}$$

Hence, the average intensity has nothing to do with random fluctuations of surface height.

Figure 1b shows the geometry for the evaluation of the two-position intensity correlation function. Two line receivers are placed at different depths but the same horizontal positions. The depth difference or separation is d. The ranges R_1 and R_2 and the corresponding scattering angles θ_1 and θ_2 are defined in the figure. The range R_s and the corresponding angle θ are used to define the midpoint between the two receivers. Hence, R_1, R_2, θ_1, and θ_2 can be expressed in terms of R_s, θ, and d as

$$\theta_1 = \theta - \sin^{-1}(d\cos\theta/2R_1) \tag{11}$$

$$\theta_2 = \theta + \sin^{-1}(d\cos\theta/2R_2) \tag{12}$$

and

$$R_{1,2} = [R_s^2 + (d/2)^2 \mp d\,R_s\sin\theta]^{1/2} \quad . \tag{13}$$

These equations will be used in the following sections.

III. SCINTILLATION INDEX

Since the scintillation index is related to a limiting value of the two-position intensity correlation function $\langle I_1 I_2\rangle$, the derivation in this section starts with $\langle I_1 I_2\rangle$. Only the detailed results of the scintillation index are presented in this section. Those of the two-position intensity correlation function will be given in the next section.

The derivation starts with

$$\langle I_1 I_2 \rangle = \langle |p_1|^2 |p_2|^2 \rangle$$

$$= \int\int\int\int_{-\infty}^{\infty} dx_1 dx_2 dx_3 dx_4 \exp\{-i[(x_1^2 - x_2^2)/x_{f1}^2 + (x_3^2 - x_4^2)/x_{f2}^2 + 2\alpha_1(x_1 - x_2) + 2\alpha_2(x_3 - x_4)]\} \times \langle \exp\{-i[2\gamma_1(\zeta(x_1) - \zeta(x_2)) + 2\gamma_2(\zeta(x_3) - \zeta(x_4))]\} \rangle \quad (14)$$

The ensemble average can be reduced to

$$\exp(-4\langle\zeta^2\rangle H) = \exp\{-4\langle\zeta^2\rangle[\gamma_1^2 + \gamma_2^2 - \gamma_1^2 C_\zeta(x_1 - x_2) - \gamma_2^2 C_\zeta(x_3 - x_4) + \gamma_1\gamma_2(C_\zeta(x_1 - x_3) - C_\zeta(x_2 - x_3) - C_\zeta(x_1 - x_4) + C_\zeta(x_2 - x_4))]\} \quad (15)$$

Here, $\langle\zeta^2\rangle$ is the mean square fluctuation of the surface height and $C_\zeta(x)$ is the normalized correlation function of the surface height fluctuation. In Eqs. (14) and (15), x_{f1}, x_{f2}, γ_1, and γ_2 are defined in Eqs. (7) and (9) for the two receiving points, respectively. By considering the following variable transformation with unit Jacobian:

$$\begin{bmatrix} x_1 \\ x_2 \\ x_3 \\ x_4 \end{bmatrix} = \begin{bmatrix} 1 & 1 & 1 & 1 \\ 1 & -1 & 1 & -1 \\ 1 & -1 & -1 & 1 \\ 1 & 1 & -1 & -1 \end{bmatrix} \begin{bmatrix} t \\ P/2 \\ S/2 \\ q/4 \end{bmatrix} \quad (16)$$

the integrations with respect to t and q can be easily completed. The result is

$$\langle I_1 I_2 \rangle = \frac{4\pi\ell^4\Lambda_1\Lambda_2}{\Lambda_1 + \Lambda_2} \int\int_{-\infty}^{\infty} d\bar{P}d\bar{S} \exp\{-i[2\bar{P}\bar{S}/(\Lambda_1 + \Lambda_2) + \bar{P}B']\} \times \exp[-4\langle\zeta^2\rangle H(\bar{S}, \bar{P})] \quad (17)$$

with

$$H(\bar{S},\bar{P}) = \gamma_1^2 + \gamma_2^2 - \gamma_1^2 C_\zeta(2\bar{P}\ell\eta) - \gamma_2^2 C_\zeta(2\bar{P}\ell(1-\eta))$$
$$+ \gamma_1\gamma_2[C_\zeta((\bar{P}+\bar{S})\ell) - C_\zeta(\bar{P}\ell(2\eta-1) - \bar{S}\ell) - C_\zeta(\bar{P}\ell(2\eta-1) + \bar{S}\ell) \quad (18)$$
$$+ C_\zeta((\bar{S}-\bar{P})\ell)]$$

in terms of

$$\Lambda_{1,2} = x_{f1,2}^2/2\ell^2 \quad (19)$$

$$B' = 4\ell(\alpha_1 x_{f1}^2 - \alpha_2 x_{f2}^2)/(x_{f1}^2 + x_{f2}^2) \quad (20)$$

$$\eta = x_{f1}^2/(x_{f1}^2 + x_{f2}^2) \quad (21)$$

the $\bar{P} = P/\ell$, $\bar{S} = S/\ell$. The notation ℓ represents the characteristic length of surface height fluctuation or more precisely is the scale size of the correlation function $C_\zeta(x)$. If we define

$$\Lambda = x_f^2/2\ell^2 \quad (22)$$

and x_f and γ as in Eqs. (7) and (9) for the midpoint between the two receivers, $\langle I_1 I_2\rangle$ in Eqs. (17) and (18) can be further reduced to

$$\langle I_1 I_2\rangle = \frac{4\pi\ell^4\Lambda\Lambda_1\Lambda_2}{\Lambda_1+\Lambda_2}\int\int_{-\infty}^{\infty} dP'\,dS' \exp[-i(DP'S' + BP')] \quad (23)$$
$$\times \exp[-\Phi^2 H'(S',P')]$$

with

$$H'(S',P') = \overline{\gamma}_1^2 + \overline{\gamma}_2^2 - \overline{\gamma}_1^2 C(2P'\eta) - \overline{\gamma}_2^2 C(2P'(1-\eta))$$
$$+ \overline{\gamma}_1\overline{\gamma}_2 [C(P'+S') - C(P'(2\eta-1) - S') \tag{24}$$
$$-C(P'(2\eta-1)+S') + C(S'-P')]$$

Here,

$$D = 2\Lambda/(\Lambda_1+\Lambda_2) \tag{25}$$

$$B = \sqrt{\Lambda}\, B' \tag{26}$$

$$\overline{\gamma}_{1,2} = \gamma_{1,2}/\gamma \tag{27}$$

$$\Phi^2 = 4\langle\zeta^2\rangle\gamma^2 \tag{28}$$

and

$$C(x) = C_\zeta(x x_f/\sqrt{2}) \tag{29}$$

Also, the new integration variables are $P' = \overline{P}/(\Lambda)^{1/2}$ and $S' = \overline{S}/(\Lambda)^{1/2}$. From Eq. (28), Φ is an indicator of scattering strength.

Equations (23) and (24) will be used for evaluating the two-position intensity correlation function. The rest of this section is devoted to the computations of the scintillation index. When positions 1 and 2 coincide, B = 0, η = 1/2, and D = 1, as can be seen in Eqs. (20), (21), and (25), respectively. In this situation, Eqs. (23) and (24) become

$$\langle I^2\rangle = 2\pi k^4\Lambda^2\int\int_{-\infty}^{\infty} dP'\,dS' \exp(-iP'S')\exp[-\Phi^2 H'(S',P')] \tag{30}$$

with

$$H'(S',P') = 2 - 2C(P') - 2C(S') + C(P'+S') + C(P'-S') \tag{31}$$

The fact that the normalized correlation function $C_\zeta(x)$ or $C(x)$ is an even function has been used. It is noted that the integration in Eq. (30) must result in a real number for $\langle I^2\rangle$ although the integrand is complex. Hence, this integration possesses inversion symmetry with respect to both P' and S'. Therefore, Eq. (30) can be rewritten as

$$\langle I^2\rangle/\langle I\rangle^2 = \frac{2}{\pi} Re \int_0^\infty\int dP'dS' \exp(-iP'S') \exp[-\Phi^2 H'(S',P')] \qquad (32)$$

where $\langle I\rangle$ given in Eq. (10) is used and Re stands for "the real part of."

To numerically evaluate the integration in Eq. (32), the integration area is divided into three regions (I, II, III) as shown in Figure 2. The dimensions defining the three parts L, L_1, L_2 and L_3, follow the relations

$$L_2 = L_1 + \sqrt{2}L \qquad (33)$$

and

$$L_3 = \sqrt{2}L_1 + L \qquad (34)$$

The sizes of L and L_1 will be defined later. In these three integration regions, different approximations will be used for numerical computations. If the physical size of L is much larger than the scale size of the correlation of ζ, i.e., $C(L) \ll 1$, the integration for $\langle I^2\rangle/\langle I\rangle^2$ over region I becomes

$$(\langle I^2\rangle/\langle I\rangle^2)_I = \frac{2}{\pi} Re \iint_{(I)} dP'dS' \exp(-iP'S') \exp[-\Phi^2 H'(S',P')] \qquad (35)$$

with

$$H'(S',P') = 2 + C(P'-S'). \qquad (36)$$

If the variable transformations $x = (S' + P')/2$ and $y = P' - S'$ are used, it is easy to obtain

$$P'S' = x^2 - y^2/4 . \tag{37}$$

With the phase factor $y^2/4$ in the integrand of Eq. (35), the contribution to the integration is negligible for large y. Hence, if L_1 is chosen so that $L_1^2/4 \gg 2\pi$, Eq. (35) can be approximated by

$$(\langle I^2\rangle/\langle I\rangle^2)_I = \frac{2}{\pi} Re \int_{L_2/\sqrt{2}}^{\infty} dx \int_{-\infty}^{\infty} dy \exp[-i(x^2 - y^2/4)] \times \exp[-\Phi^2(2 + C(y))] . \tag{38}$$

Next, if Φ is not extremely large, we expect that $1 - \exp[-\Phi^2 C(y)]$ decreases very fast with y. Therefore,

$$(\langle I^2\rangle/\langle I\rangle^2)_I = \frac{2}{\pi} Re\, \xi_2 \{2\xi_1 - \int_{-\infty}^{\infty} dy [1 - \exp(-\Phi^2 C(y))]\} \times \exp(-2\Phi^2) \tag{39}$$

where

$$\xi_1 = \sqrt{\frac{\pi}{2}}(1 + i) \tag{40}$$

and ξ_2 is a Fresnel integral as

$$\xi_2 = \int_{L_2/\sqrt{2}}^{\infty} dx \exp(-ix^2) . \tag{41}$$

The integrations in Eqs. (39) and (41) can be easily completed for

$< \langle I^2\rangle/\langle I\rangle^2)_I$.

For region II, we have

$$(\langle I^2\rangle/\langle I\rangle^2)_{II} = \frac{4}{\pi} Re \int_{L_1}^{\infty} dP' \int_0^L dS' \exp(-iS'P') \exp[-\Phi^2 H'(S',P')] . \quad (42)$$

Here, a factor of 2 has been included since region III covers two separate parts which result in the same integration value. Because the physical size of L is much larger than the scale size of C(x), the upper integration limit L for S' in Eq. (42) can be replaced by ∞ without significantly changing the integration result. Also, H'(S',P') can be approximated by

$$H'(S',P') = 2 - 2C(S') . \quad (43)$$

Hence, Eq. (42) becomes

$$(\langle I^2\rangle/\langle I\rangle^2)_{II} = \frac{2}{\pi} Re \int_{L_1}^{\infty} dP' \int_{-\infty}^{\infty} dS' \exp(-iS'P') \exp[-2\Phi^2(1 - C(S'))] . \quad (44)$$

It is evident that the integration with respect to S' is a Fourier transform and can be easily evaluated using the Fast Fourier Transform algorithm on a computer.

For region III, no approximation can be made. Double integrations on a computer must be performed. The contribution from region III is

$$(\langle I^2\rangle/\langle I\rangle^2)_{III} = \frac{2}{\pi} Re \left[\int_0^{L_1} dP' \int_0^{L+L_1-P'} dS' - \int_0^{L} dP' \int_{L_1}^{L+L_1-P'} dS'\right] \times \exp(-iS'P') \exp[-\Phi^2 H'(S',P')] \quad (45)$$

with H'(S',P') given in Eq. (31).

Hence, $\langle I^2\rangle/\langle I\rangle^2$ is the summation of the results in Eqs. (39), (44), and

(45). For numerical computations, the correlation function of surface height fluctuation ζ must be chosen. To illustrate the dependence of the scintillation index on the parameters Φ and Λ, a Gaussian correlation function, corresponding to a Gaussian spectrum, is used

$$C_\zeta(x) = \exp\left[-(x/\ell)^2\right] \tag{46}$$

and, hence

$$C(x') = \exp\left[-(x'\sqrt{\Lambda})^2\right]. \tag{47}$$

In numerical computations, $L = 5/\sqrt{\Lambda}$ and $L_1 = (80\pi)^{1/2}$ are used. The numerical accuracy was checked by decreasing the step sizes in the integrations until the results were not changed. Three curves are plotted in Figure 3 for the scintillation index σ versus Φ for three different Λ values of 2.58 (long-dashed), 50 (short-dashed), and 245 (solid) when the Gaussian correlation given in Eqs. (46) and (47) is used. Each curve increases with Φ and approaches unity asymptotically. In other words, the scintillation index increases with scattering strength and becomes close to one when saturation is almost reached. The wave field follows a jointly Gaussian distribution in the saturation regime. The fact that the scintillation index does not exceed unity implies that the phenomenon of focusing-defocusing does not occur. Among these three curves, the higher the value of Λ, the larger is the scintillation index. To further explore this trend, from Eqs. (7) and (22) under the assumptions $\theta_1 = \theta_s = \theta$ and $R_1 = R_s = R$, we can obtain

$$\Lambda = R/(2k\ell^2 \sin^2\theta). \tag{48}$$

It is easy to understand that a smaller ℓ value (larger Λ) leads to stronger scattering and, hence, a larger scintillation index. Also, as the range R is increased more complete evolution from phase fluctuations, which are due to rough surface scattering, into amplitude fluctuations is expected. Therefore, a larger R value (larger Λ) results in a larger scintillation index. It is noted that for $\Phi<2$, the approximations used fail. The numerical methods used will also fail for very strong scatter.

IV. TWO-POSITION CORRELATION FUNCTION

The computations for the two-position correlation function start from Eqs. (23) and (24). By using Eq. (10),

$$\langle I_1 I_2\rangle / \langle I_1\rangle\langle I_2\rangle = \frac{2\Lambda}{\pi(\Lambda_1+\Lambda_2)} Re\int_0^{\infty} dP' \int_{-\infty}^{\infty} dS' \exp[-i(DP'S'+BP')] \times \exp[-\Phi^2 H'(S',P')] \tag{49}$$

where H'(S',P') is given in Eq. (24). In obtaining Eq. (49), the symmetry with respect to P' was used. Because this integration does not possess symmetry with respect to S', the partition of the integration area is different from that for computing the scintillation index. For the integrations in Eq. (49), four regions (I through IV) are designated as shown in Figure 4. Among them, regions I and II individually have two separate sections. For simplicity in notation, we define

$$E = 2Re\int_0^{\infty} dP' \int_{-\infty}^{\infty} dS' \exp[-i(DP'S'+BP')] \times \exp[-\Phi^2 H'(S',P')] \tag{50}$$

and, hence

$$\langle I_1 I_2 \rangle / \langle I_1 \rangle \langle I_2 \rangle = \frac{\Lambda E}{\pi (\Lambda_1 + \Lambda_2)}. \tag{51}$$

The dimensions L, L_1, L_2, and L_3 in Figure 4 are the same as those in Figure 2.

The approximation used for region 1 is the same as that for region I in Figure 2. It results in

$$E_I = 2Re\,(F \cdot G) \tag{52}$$

where

$$F = \left(\frac{\pi}{2D}\right)^{1/2} \exp\left(-iB^2/4D\right)\{[1 - C_1(u) - C_1(v)] - i[1 - S_1(u) - S_1(v)]\} \tag{53}$$

and

$$\begin{aligned} G = \exp\left[-\Phi^2\left(\bar{\gamma}_1^2 + \bar{\gamma}_2^2\right)\right]\{&\left(\frac{2\pi}{D}\right)^{1/2}(1+i)\exp\left(iB^2/4D\right) \\ &-2\int_0^{\infty} dy\,[1 - \exp\left(-\Phi^2 \bar{\gamma}_1 \bar{\gamma}_2 C(y)\right)]\}. \end{aligned} \tag{54}$$

The approximation for region II here is again the same as that for region II in Figure 2. The contribution from this region is

$$\begin{aligned} E_{II} = \frac{2}{D} Re \int_{DL_3}^{\infty} dS' \int_{-\infty}^{\infty} dP' \exp\left(-iP'S'\right) \\ \times \{\cos\left(P'B\right)\,[\exp(-\Phi^2[\bar{\gamma}_1^2 + \bar{\gamma}_2^2 - \bar{\gamma}_1^2 C(2P'\eta) - \bar{\gamma}_2^2 C(2P'(1-\eta))]) \\ -\exp\left(-\Phi^2\left(\bar{\gamma}_1^2 + \bar{\gamma}_2^2\right)\right)]\}. \end{aligned} \tag{55}$$

Again, the algorithm of the Fast Fourier Transform can be used for the integration with respect to P'. No approximation can be made for region III; its contribution

is

$$E_{III} = 4Re\left[\int_{L}^{L_1} dP' \int_{0}^{L+L_1-P'} dS' + \int_{0}^{L} dP' \int_{0}^{L_1} dS'\right] \exp(-iDP'S') \times \cos(P'B) \exp\left[-\Phi^2 H'(S', P')\right] \tag{56}$$

Here, H'(S',P') was defined by Eq. (24). Finally, for region IV the two-fold integration cannot be simplified. However, H'(S',P') can be reduced to produce

$$E_{IV} = 2Re\int_{L_1}^{\infty} dP' \int_{-L-(P'-L_1)(2\eta-1)}^{L+(P'-L_1)(2\eta-1)} dS' \exp(-iDP'S' - iP'B) \times \exp\left\{-\Phi^2\left[\bar{\gamma}_1^2 + \bar{\gamma}_2^2 - \bar{\gamma}_1\bar{\gamma}_2\left(C(P'(2\eta-1) - S') + C(P'(2\eta-1) + S')\right)\right]\right\} \tag{57}$$

This two-fold integration is quite time consuming on a computer, especially when η approaches 1/2. It is noted that E_{IV} is equal to E_{II} when $\eta = 1/2$. This equality can be used to check the accuracy of E_{IV}. Combining Eqs. (52), (55), (56), and (57), we can obtain E as

$$E = E_I + E_{II} + E_{III} + E_{IV} \tag{58}$$

and thence $\langle I_1 I_2\rangle / \langle I_1\rangle\langle I_2\rangle$ from Eq. (51).

To describe realistic ocean surface fluctuations, the D/P spectrum [13] is used at low wave numbers and the empirical spectral model of Pierson and Stacy [15] and Pierson [16] at high wave numbers. This combined spectrum has an approximate dependence on the inverse cube of the wave number over a wave number span that is determined by wind speed and vanishes outside this region. In this spectrum, both scale size ℓ and mean-square fluctuation $\langle\zeta^2\rangle$ are controlled by the wind speed at the ocean surface. Two normalized D/P correlation functions are depicted in Figure 5 for wind speeds of 10 m/s (solid curve) and 15 m/s (dashed

curve). Side lobes for both curves can be seen. The scale size ℓ is defined as the length at which the correlation drops to one-half of the maximum value. Therefore, we have ℓ = 9.27 m and 22.61 m for wind speeds of 10 m/s and 15 m/s, respectively. Also, the mean-square fluctuations are $\langle\zeta^2\rangle$ = 1.08 m^2 and 5.38 m^2, respectively, for the lower and higher wind speeds.

In numerical computations, we again choose $L = 5/\sqrt{\Lambda}$ and $L_1 = (80\pi)^{1/2}$ Other parameters are θ = 10° and k = 4π (frequency = 3 kHz). Two values for $R_i = R_s = R$ at 1 km at 10 km will be used. Figure 6 shows the results for the normalized two-position intensity correlation function $\langle I_1 I_2\rangle/\langle I_1\rangle\langle I_2\rangle$ as a function of the separation d between the two receivers for various situations.

The four solid curves labelled by A, B, C, and D show the results for the D/P correlations with: (A) R = 1 km and wind speed = 10 m/s,

(B) R = 1 km and wind speed = 15 m/s,

(C) R = 10 km and wind speed = 10 m/s,

and (D) R = 10 km and wind speed = 15 m/s.

For comparison, two dashed curves are plotted for the Gaussian correlation with (A') R = 1 km and (C') R = 10 km. The scale size of the Gaussian correlation is set at 9.27 m and mean-square fluctuation $\langle\zeta^2\rangle$ is 1.08 m^2 which correspond to the wind speed at 10 m/s in the D/P correlation. The comparison between curves A and B shows that for weak scattering the two-position intensity correlation is higher for a higher wind speed. When the range R increases, phase fluctuations of the scattered wave can evolve into amplitude fluctuations more completely and, hence, the curves for the intensity correlation become higher. In the case of R = 10 km, although the scintillation index at a wind speed of 15 m/s is higher than that at 10 m/s, the intensity correlation decreases faster with separation between the two

receivers. The comparison between curves A and A′ and that between curves C and C′ show that if all other parameters are the same, the Gaussian spectrum leads to weaker scattering. Because forward scatter in the Kirchhoff approximation is governed by local specular reflection from properly oriented "facets" on the surface, the mean-square surface slope determines the area of the surface that contributes effectively to scattering. The quasi power law dependence of the D/P spectrum yields higher mean-square surface slopes, and, hence, stronger scattering than does the Gaussian spectrum. It is noted that curves A, B, C, and C′ are almost parallel, indicating that the correlation lengths in these cases are about the same. Since curve D is steeper than curve C, the correlation length is shorter and scattering is stronger in the case of D. For the same reason, the scattering in the case of A′ is very weak.

V. TWO-POSITION COHERENCE FUNCTION

As discussed earlier in this paper, the two-position coherence function carries information on phase fluctuations. The derivations start with

$$\begin{aligned} \langle (p_1 p_2^*)^2 \rangle = \iiiint_{-\infty}^{\infty} dx_1 dx_2 dx_3 dx_4 \exp\{-i[(x_1^2 + x_3^2)/x_{f1}^2 \\ - (x_2^2 + x_4^2)/x_{f2}^2 + 2\alpha_1(x_1 + x_3) - 2\alpha_2(x_2 + x_4)]\} \\ \times \langle \exp\{-i[2\gamma_1(\zeta(x_1) + \zeta(x_3)) - 2\gamma_2(\zeta(x_2) + \zeta(x_4))]\} \rangle \end{aligned} \tag{59}$$

After using the variable transformation in Eq. (16), the integrations with respect to t and q can be completed using the method of stationary phase to produce

$$\langle (p_1 p_2^*)^2 \rangle = 2\pi x_{f1} x_{f2} \ell^2 \exp\left[-2i(\alpha_2^2 x_{f2}^2 - \alpha_1^2 x_{f1}^2)\right]$$
$$\times \int_0^\infty d\bar{P} \int_{-\infty}^{\infty} d\bar{S} \exp\{-i[(\bar{P}+\bar{S})^2/4\Lambda_1 - (\bar{P}-\bar{S})^2/4\Lambda_2]\} \quad (60)$$
$$\times \exp\left[-4\langle\zeta^2\rangle H(\bar{S},\bar{P})\right]$$

where

$$H(\bar{S},\bar{P}) = \gamma_1^2 + \gamma_2^2 + \gamma_1^2 C_\zeta(\bar{P}+\bar{S}) + \gamma_2^2 C_\zeta(\bar{S}-\bar{P})$$
$$-\gamma_1\gamma_2\left[C_\zeta(\bar{P}+\overline{q_o}/2) + C_\zeta(\bar{S}+\overline{q_o}/2) + C_\zeta(\overline{q_o}/2-\bar{S})\right. \quad (61)$$
$$\left.+C_\zeta(\overline{q_o}/2-\bar{P})\right]$$

with

$$\overline{q_o} = 4\ell^2(\alpha_2\Lambda_2 - \alpha_1\Lambda_1) \quad (62)$$

Further normalization of $\bar{P}$ *and* $\bar{S}$ does not simplify the computations. Again, for simplicity of notation the two-fold integration A is defined by

$$A = \int_0^\infty d\bar{P} \int_{-\infty}^{\infty} d\bar{S} \exp\{-i[(\bar{P}+\bar{S})^2/4\Lambda_1 - (\bar{P}-\bar{S})^2/4\Lambda_2]\} \quad (63)$$
$$\times \exp\left[-4\langle\zeta^2\rangle H(\bar{S},\bar{P})\right]$$

Hence, the normalized two-position coherence function is

$$\langle (p_1 p_2^*)^2 \rangle / \langle I_1 \rangle \langle I_2 \rangle = \frac{A}{\pi\sqrt{\Lambda_1\Lambda_2}} \exp\left[-2i(\alpha_2^2 x_{f2}^2 - \alpha_1^2 x_{f1}^2)\right] \quad (64)$$

Five regions can be identified for computing A as shown in Figure 7. Regions II and V individually include two areas. The dimensions, L', L_1', L_2', and L_3' are clearly shown in the figure. They are defined by

$$L_2' = L_1' + \sqrt{2}\,L' \tag{65}$$

and

$$L_3' = \sqrt{2}\,L_1' + L'. \tag{66}$$

The choice of L' and L_1' must satisfy the inequalities $L' - \overline{q_o}/2 > > 1$ and $L'^2_1/4\Lambda_j > > 2\pi$ for both j = 1 and 2, respectively. For the contributions from regions I and IV, the approximation used for region I in Figure 2 can be applied. The results are

$$A_I = \exp\left[-\Phi^2(\overline{\gamma_1^2} + \overline{\gamma_2^2})\right] g_1\{(2\pi\Lambda_2)^{1/2}(1+i) - 2\int_o^\infty dy\,[1 - \exp(-\Phi^2\overline{\gamma_2^2}C_\zeta(y))]\} \tag{67}$$

and

$$A_{IV} = \exp\left[-\Phi^2(\overline{\gamma_1^2} + \overline{\gamma_2^2})\right] g_2\{(2\pi\Lambda_1)^{1/2}(1-i) - 2\int_o^\infty dy\,[1 - \exp(-\Phi^2\overline{\gamma_1^2}C_\zeta(y))]\} \tag{68}$$

where

$$g_1 = (\pi\Lambda_1/2)^{1/2}\{[1/2 - C_1(L_2'/\sqrt{\pi\Lambda_1})] - i[1/2 - S_1(L_2'/\sqrt{\pi\Lambda_1})]\} \tag{69}$$

and

$$g_2 = (\pi\Lambda_2/2)^{1/2}\{[1/2 - C_1(L_2'/\sqrt{\pi\Lambda_2})] + i[1/2 - S_1(L_2'/\sqrt{\pi\Lambda_2})]\} \tag{70}$$

To obtain the contributions from regions II and V, the approximation used for region II in Figure 2 can be utilized to produce the combined result

$$A_{II\,V} = A_{II} + A_V$$

$$= \frac{4\Lambda_1\Lambda_2}{\Lambda_1+\Lambda_2} \int_{L_3(\Lambda_1+\Lambda_2)/2\Lambda_1\Lambda_2}^{\infty} d\bar{P} \exp\left[-i\Lambda_1\Lambda_2(\Lambda_2-\Lambda_1)\,\bar{P}^2/(\Lambda_1+\Lambda_2)^2\right]$$

$$\times \int_{-\infty}^{\infty} d\bar{S} \exp(-i\bar{P}\bar{S}) \exp\left[-i(\Lambda_2-\Lambda_1)\,\bar{S}^2/(4\Lambda_1\Lambda_2)\right] \tag{71}$$

$$\times \left(\exp\{-\Phi^2[\bar{\gamma}_1^2+\bar{\gamma}_2^2-\overline{\gamma_1\gamma_2}\,(C_\zeta(\bar{S}+\bar{q}_o/2)+C_\zeta(\bar{S}-\bar{q}_o/2))]\}\right.$$

$$\left.-\exp\{-\Phi^2(\bar{\gamma}_1^2+\bar{\gamma}_2^2)\}\right).$$

Again, the FFT algorithm can be used for the integration with respect to $\bar{S}$. Finally, without any approximation the contribution from region III is

$$A_{III} = \left[\int_0^{L'+L_3'} d\bar{P} \int_{-(L'+L_3'-\bar{P})}^{L'+L_3'-\bar{P}} d\bar{S} - 2\int_{L_3'}^{L'+L_3'} d\bar{P} \int_{-(L'+L_3'-\bar{P})}^{L'+L_3'-\bar{P}} d\bar{S}\right] \tag{72}$$

$$\times \exp\{-i[(\bar{P}+\bar{S})^2/4\Lambda_1-(\bar{P}-\bar{S})^2/4\Lambda_2]\}\exp\left[-\Phi^2 H'(\bar{S},\bar{P})\right]$$

where $H'(\bar{S},\bar{P})$ is the same as $H(\bar{S},\bar{P})$ in Eq. (61) except that γ_1 and γ_2 are replaced by $\bar{\gamma}_1$ and $\bar{\gamma}_2$, respectively. The normalized two-position coherence function can be obtained from the equality $A = A_I + A_{IV} + A_{II\,V} + A_{III}$ and Eq. (64).

The same parameter values as before are used for numerical evaluation of the normalized two-position coherence function. L' and L'_1 are chosen so that $L' - \bar{q}_o/2 = 5$ and $L_1' = (80\pi\Lambda)^{1/2}$. Figure 8 shows the absolute values of the

normalized two-position coherence function $|\langle(p_1p_2^*)^2\rangle|/\langle I_1\rangle\langle I_2\rangle|$ as a function of the separation d for various situations which are the same as those in Figure 6. Each curve drops from its maximum value, which is $\langle I^2\rangle/\langle I\rangle^2$, to zero. All the letters indicate the same cases, respectively, as those in Figure 6. The shorter coherence lengths in the cases of B and D when compared with the cases of A and C confirm that the scattering at wind speed 15 m/s is stronger. Apparently, phase fluctuations play an important role in determining the size of coherence length. Curves A' and C' show that the coherence lengths in the case of the Gaussian spectrum are about the same as those in the case of D/P spectrum when scattering is weak and are smaller when scattering is stronger.

As discussed in section I, when scattering is weak, the ratio between the absolute value of the two-position coherence function and the two-position intensity correlation describes the fluctuation of the relative phase between the two positions [see Eq. (5)]. Since the scintillation index is 0.52 in the case when R = 1 km and the wind speed is 10 m/s in the D/P spectrum, Eq. (5) must be approximately true. By using Eq. (5), the root-mean-square of the fluctuation of relative phase, i.e., $\langle(S_1 - S_2)^2\rangle^{1/2}$, is plotted for this case in Figure 9. The fluctuation of the relative phase almost reaches 2.25 (radian) at d = 17.5 cm, which is only 0.35 times a wavelength.

VI. CONCLUSIONS

Three types of fourth moments of forward-scattered acoustic waves from a randomly-rough ocean surface have been evaluated. The first is the scintillation index which characterizes the intensity fluctuations of the scattered wave. The second is the two-position intensity correlation function. It indicates the spatial correlation of the intensity. The third is the two-position coherence

function which carries information on phase fluctuations of the scattered waves. Particularly, when the scattering is not strong, the ratio of the absolute value of the two-position coherence function over the two-position intensity correlation function exactly describes the mean-square fluctuation of the relative phase between two observation positions.

The Fresnel-corrected Kirchhoff approximation was used to obtain integral expressions for the fourth moments. Various approximation techniques were developed for numerically evaluating the integrals. The approximations and numerical methods are not applicable, however, for treating the very weak or extremely strong scattering regimes. Two types of power spectra for the surface height fluctuation were considered: a Gaussian spectrum and the Donelan/Pierson spectrum which is an empirical model based on ocean wave measurements. The D/P spectrum resulted in stronger scattering than the Gaussian spectrum for the same values of Λ and Φ which was attributed to the greater mean-square surface slope obtained with the D/P spectrum. The two-position coherence function was found to decay much more rapidly with displacement between receivers than the intensity correlation function. For weak scattering, this led to large relative phase fluctuations between two vertically displaced observation points.

ACKNOWLEDGEMENT

The numerical computations were performed on computers by George Fennemore, who is a senior in the Department of Mathematics at The Pennsylvania State University. This research was sponsored by the Office of Naval Research and the Office of Naval Technology.

REFERENCES

1. B. J. Kachoyan and C. Macaskill, "Acoustic scattering from an arbitrary rough surface," J. Acoust. Soc. Am., 82, pp. 1720-1726 (1987).

2. E. I. Thorsos, "The validity of the Kirchhoff approximation for rough surface scattering using a Gaussian roughness spectrum," J. Acoust. Soc. Am., 83, pp. 78-92 (1988).

3. D. R. Jackson, D. P. Winebrenner, and A. Ishimaru, "Comparison of perturbation theories for rough-surface scattering," J. Acoust. Soc. Am., 83, pp. 961-969 (1988).

4. C. Macaskill and B. J. Kachoyan, "Numerical evaluation of the statistics of acoustic scattering from a rough surface," J. Acoust. Soc. Am., 84, pp. 1826-1835 (1988).

5. A. Wirgin, "Scattering from hard and soft corrugated surfaces: Iterative corrections to the Kirchhoff approximation through the extinction theorem," J. Acoust. Soc. Am., 85, pp. 670-679 (1989).

6. J. J. McCoy, "Shadowing by randomly rough surfaces," J. Acoust. Soc. Am., 86, pp. 1523-1529 (1989).

7. H. Faure-Geors and D. Maystre, "Improvement of the Kirchhoff approximation for scattering from rough surfaces," J. Opt. Soc. Am. A, 6, pp. 532-546 (1989).

8. O. I. Yordanov and M. A. Michalev, "Statistics of specular points on a non-Gaussian random surface," J. Opt. Soc. Am. A, 6, pp. 1578-2583 (1989).

9. C. Eftimiu, "Modified Wiener-Hermite expansion in rough-surface scattering," J. Opt. Soc. Am. A, 6, pp. 1584-1594 (1989).

10. M. J. Kim, J. C. Dainty, A. T. Friberg, and A. J. Sant, "Experimental study of enhanced backscattering from one- and two-dimensional random rough surfaces," J. Opt. Soc. Am. A, 7, pp. 569-577 (1990).

11. M. Saillard and D. Maystre, "Scattering from metallic and dielectric rough surfaces," J. Opt. Soc. Am. A, 7, pp. 982-990 (1990).

12. A. Ishimaru, Wave Propagation and Scattering in Random Media, Chapter 21, Vol. 2, Academic Press, New York (1978).

13. M. A. Donelan and W. J. Pierson, "Radar scattering and equilibrium ranges in wind-generated waves with application to scatterometry," J. Geophys. Res., 92, 4971-5029 (1987).

14. C. S. Clay and H. Medwin, Acoustical Oceanography: Principles and Applications, p. 511, John Wiley and Sons, New York (1977).

15. W. J. Pierson and R. A. Stacy, "The elevation, slope and curvature spectrum of a wind roughened sea surface," NASA Contract. Rep. CR-2247, NASA, Washington, DC (1973).

16. W. J. Pierson, "The theory and applications of ocean wave measuring systems at and below the sea surface, on the land, and from aircraft and spacecraft," NASA Contract Rep. CR-2646, NASA, Washington, DC (1976).

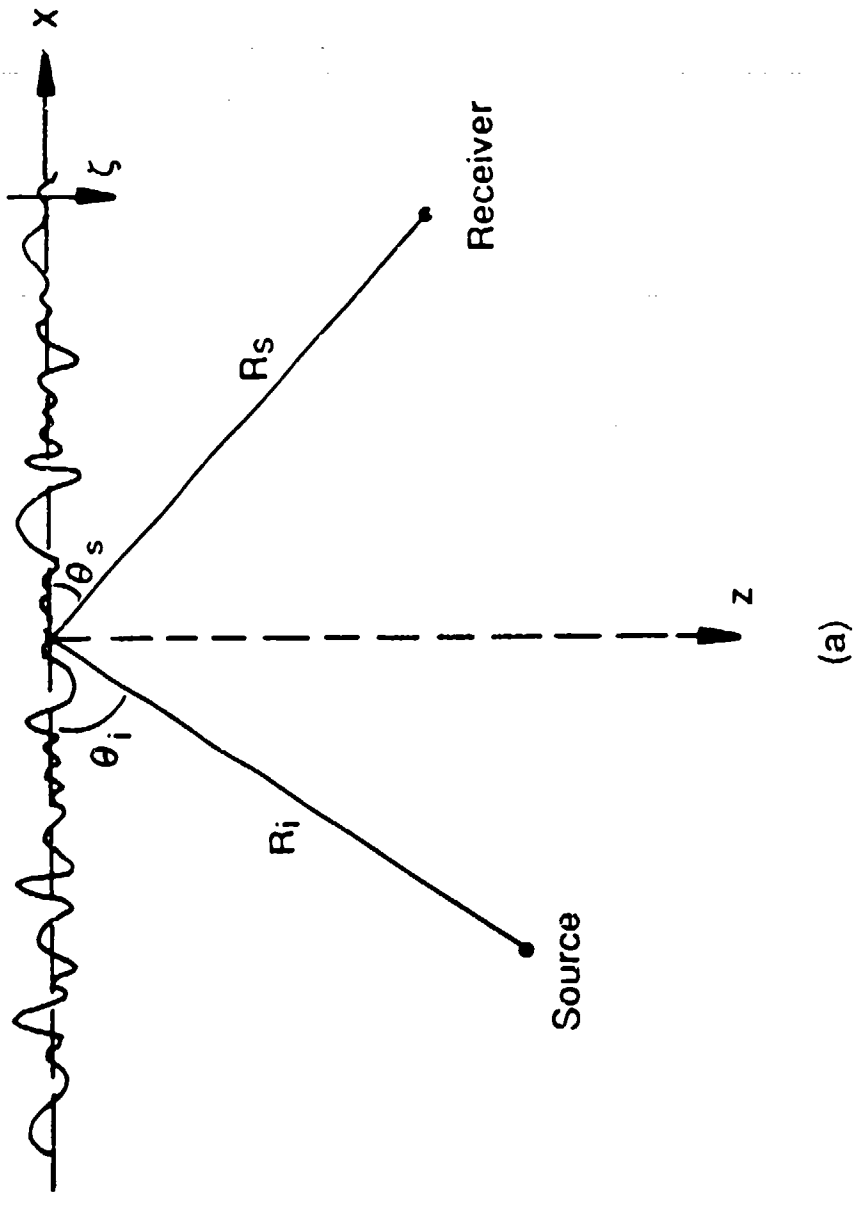

Figure 1(a). Geometry of problem. The acoustic wave is transmitted from a line source, scattered by the rough surface, and received by a line receiver. No variation for acoustic waves along the y direction is assumed. Surface height fluctuation is denoted by ζ. Part (a) shows a general geometry.

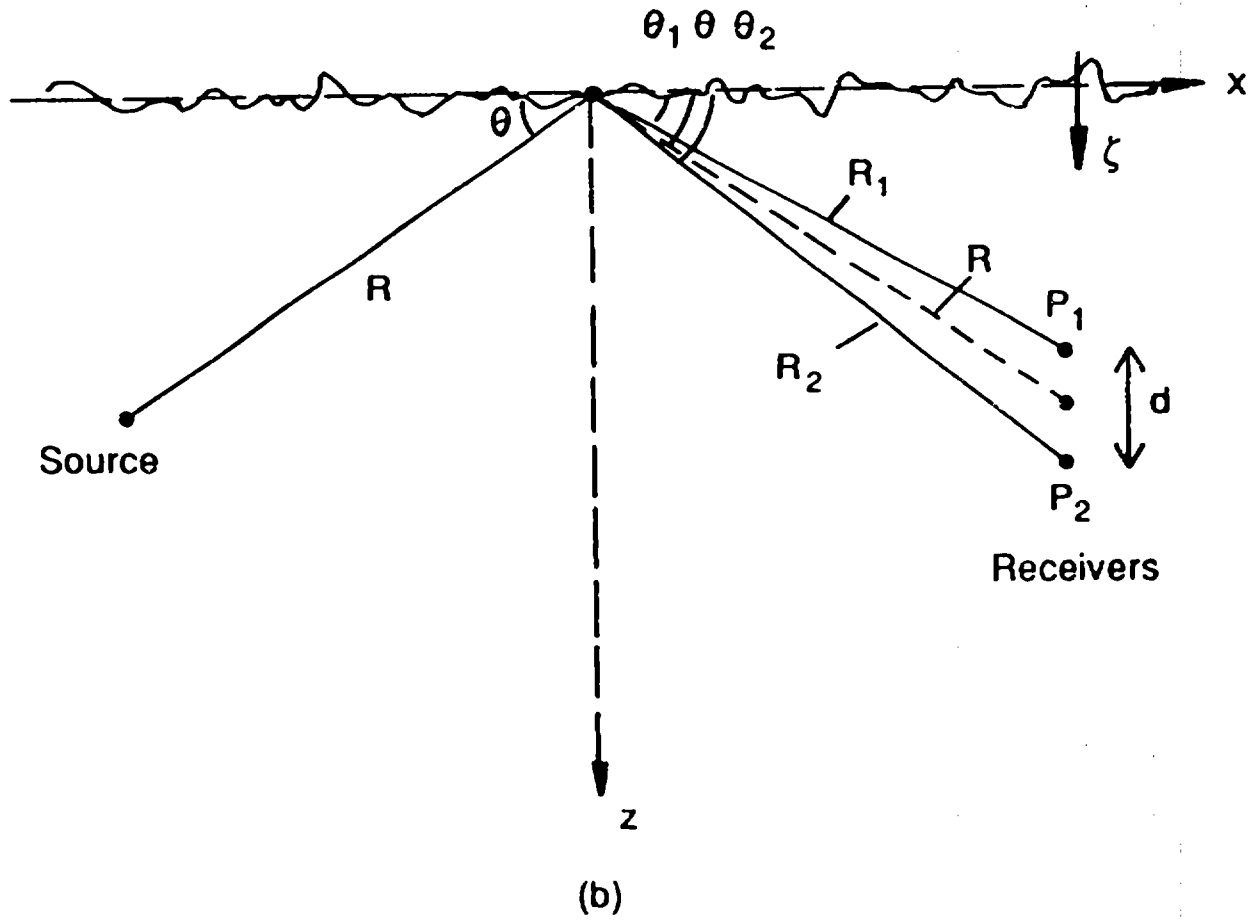

Figure 1(b). Geometry of problem. The acoustic wave is transmitted from a line source, scattered by the rough surface, and received by a line receiver. No variation for acoustic waves along the y direction is assumed. Surface height fluctuation is denoted by ζ. Part (b) demonstrates explicitly the geometry of two line receivers separated by d in depth.

9 August 1990
CCY:STM:lzh

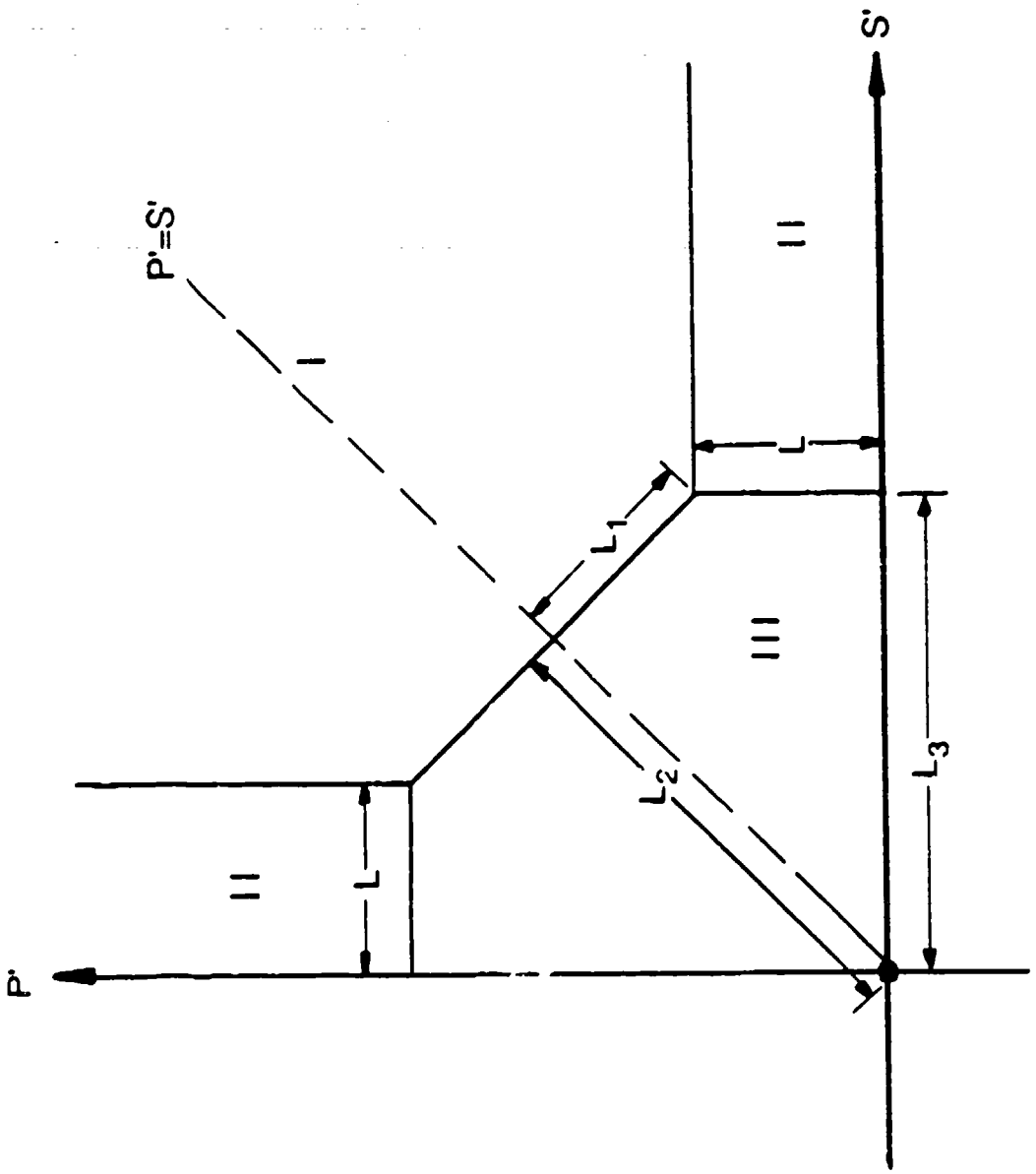

Figure 2. Three regions, I through III in the first quadrant of the S' - P' plane, are designated for the integrations for the scintillation index. Region II includes two separate areas.

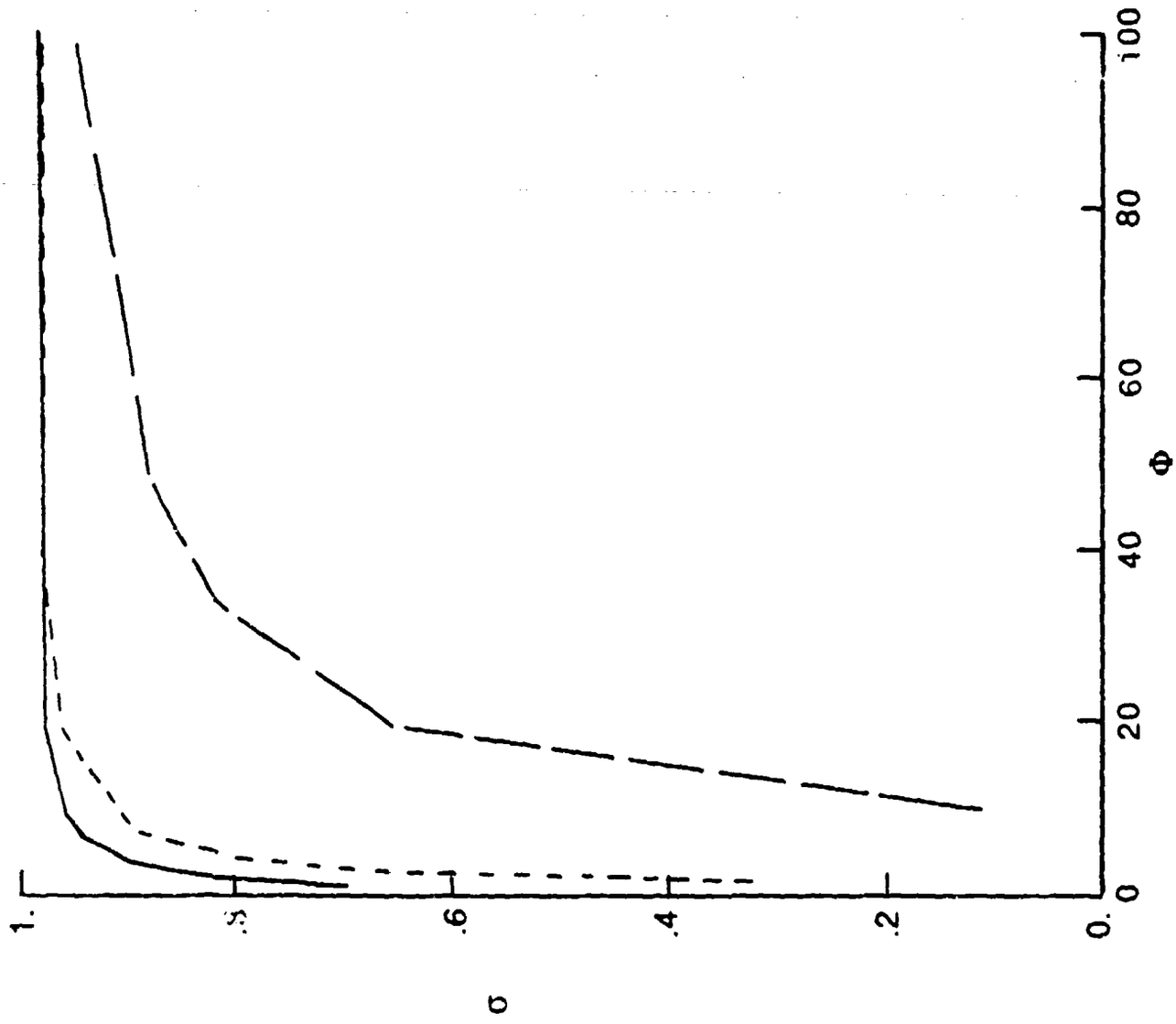

Figure 3. Scintillation index σ versus Φ in the case of the Gaussian correlation for three Λ values: Λ = 2.58 (long-dashed), 50 (short-dashed), and 245 (solid).

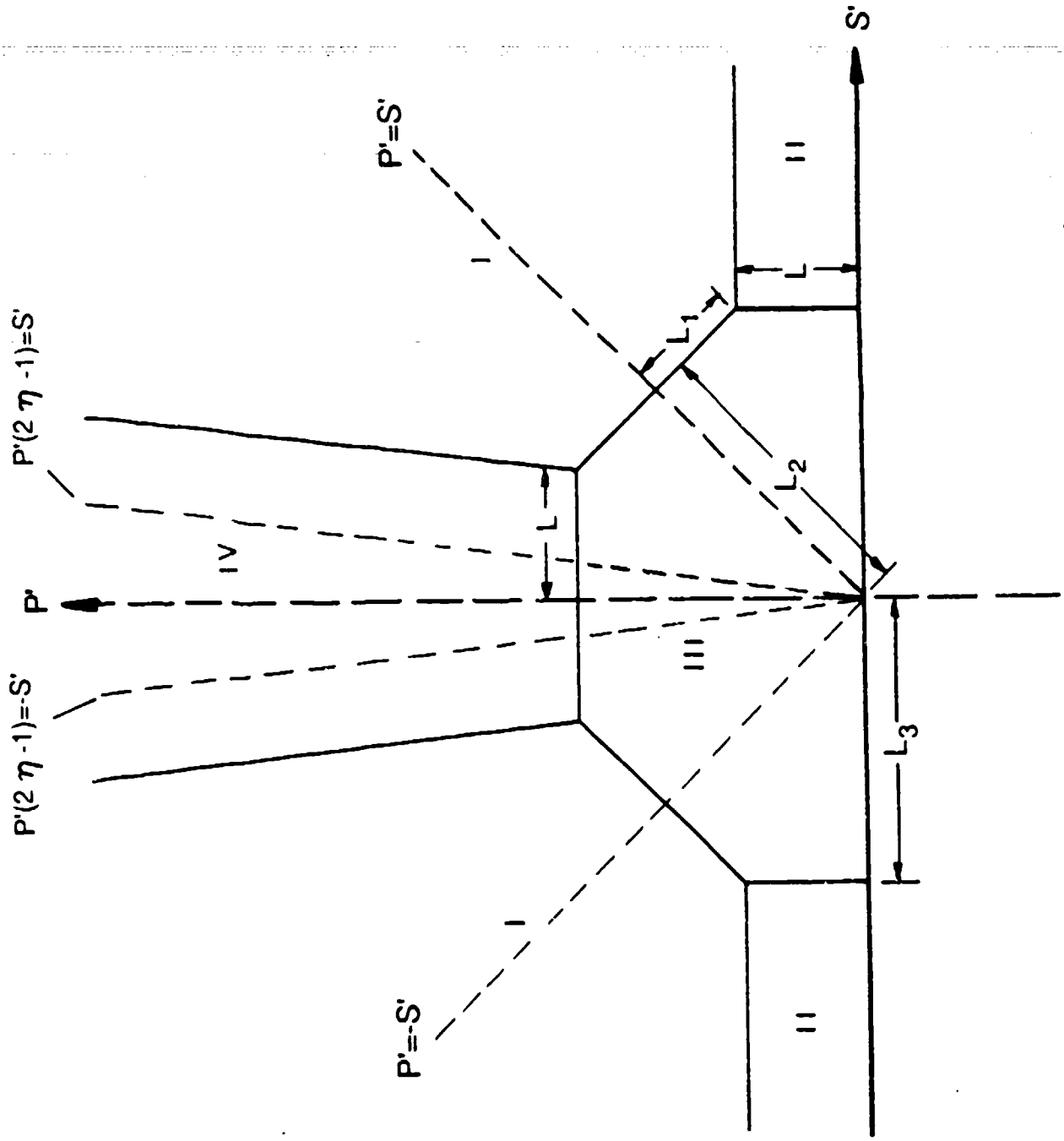

Figure 4. Four regions, I through IV in the first and second quadrants of the S' - P' plane, are designated for the integrations for the two-position intensity correlation function. Regions I and II individually include two separate areas.

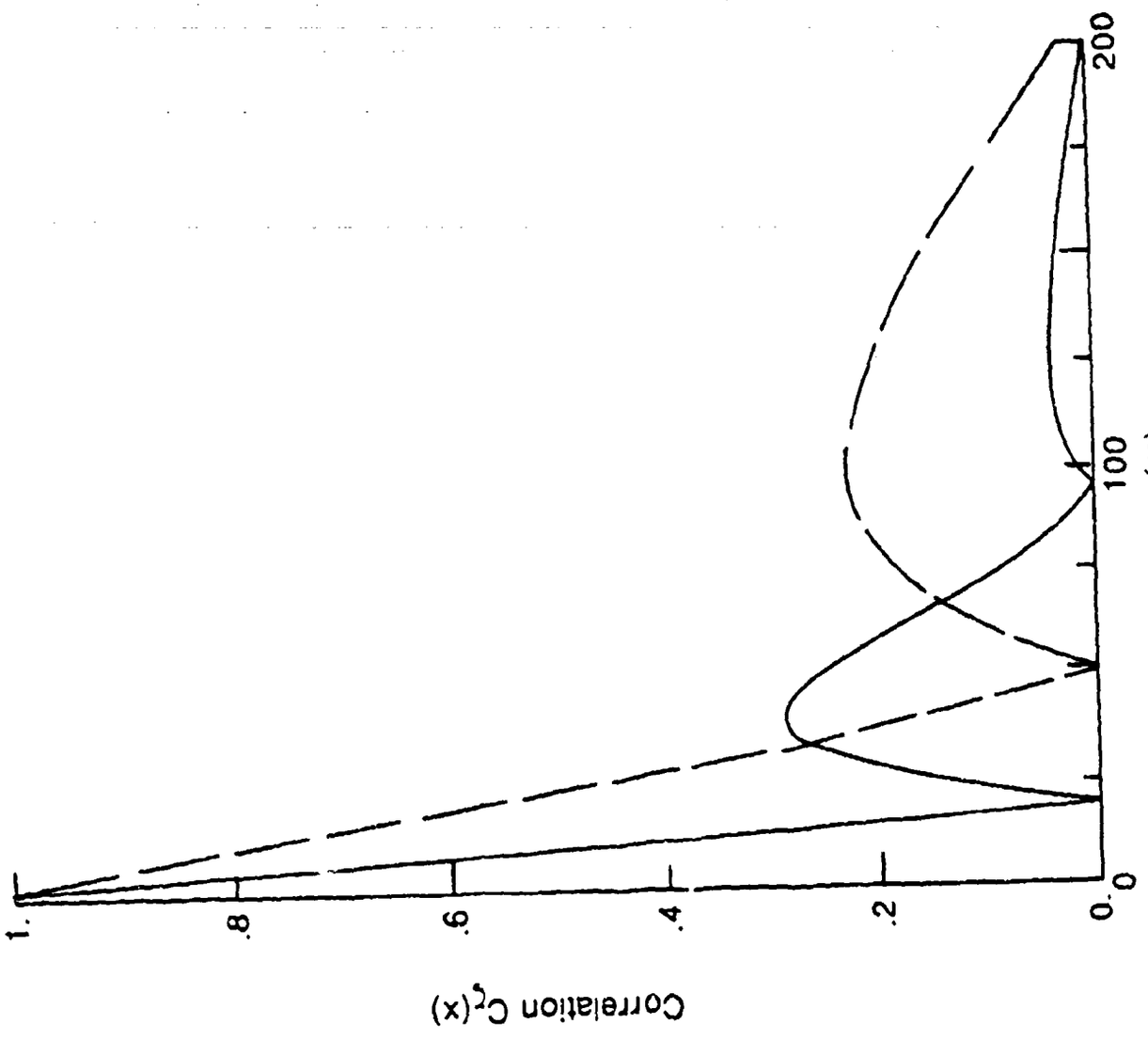

Figure 5. Correlation functions of surface height fluctuation $C_\zeta(x)$ in the Donelon/Pierson model when the wind speeds on the ocean surface are 10 m/s (solid curve) and 15 m/s (dashed curve).

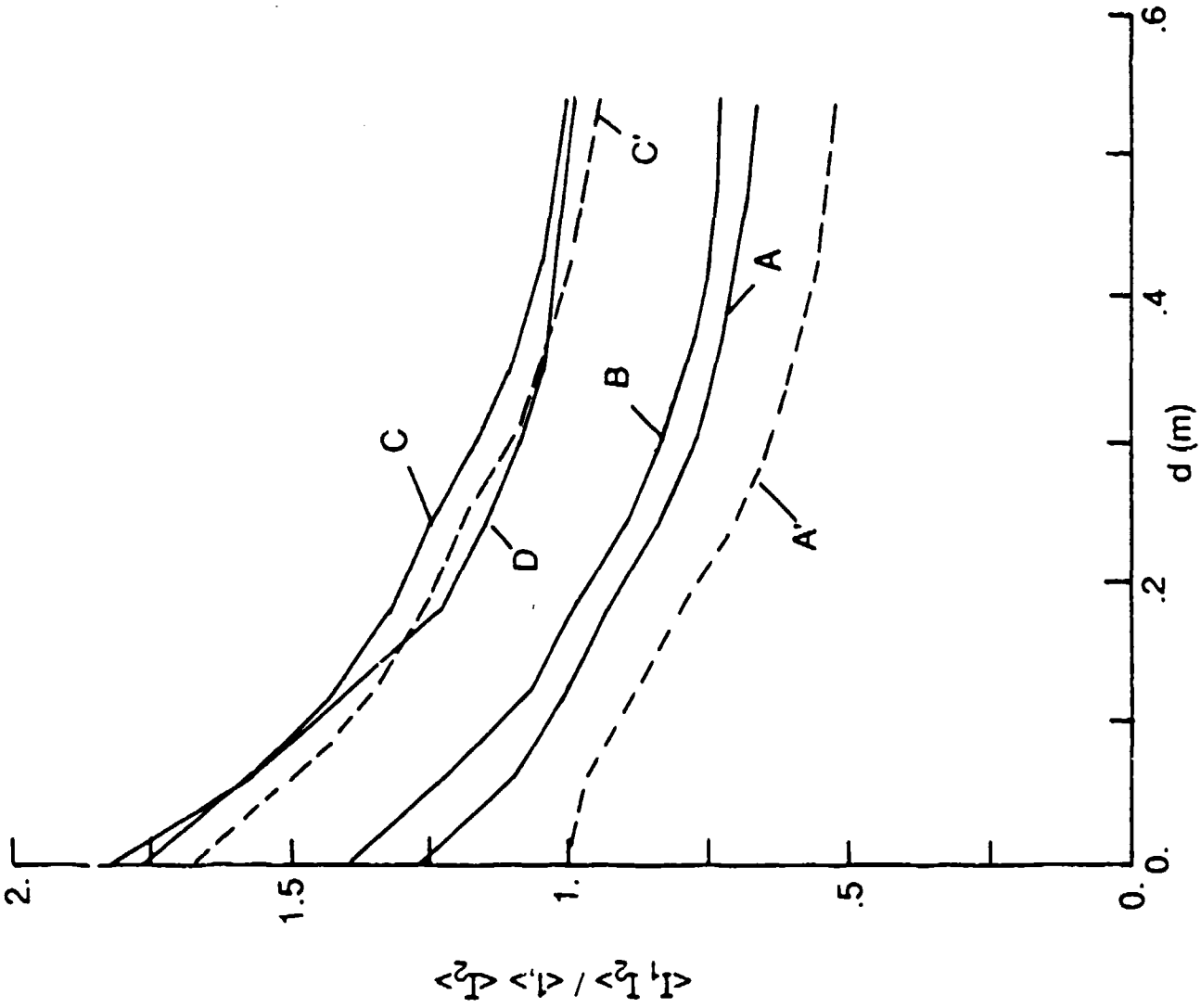

Figure 6. Normalized two-position intensity correlation versus the separation d between two receivers. The solid and dashed curves are plotted for the cases of the D/P and Gaussian spectra, respectively. The letters indicate different situations as: (A) R = 1 km and wind speed = 10 m/s, (B) R = 1 km wind speed = 15 m/s, (C) R = 10 km and wind speed = 10 m/s, (D) R = 10 km and wind speed = 15 m/s, (A') R = 1 km, and (C') R = 10 km.

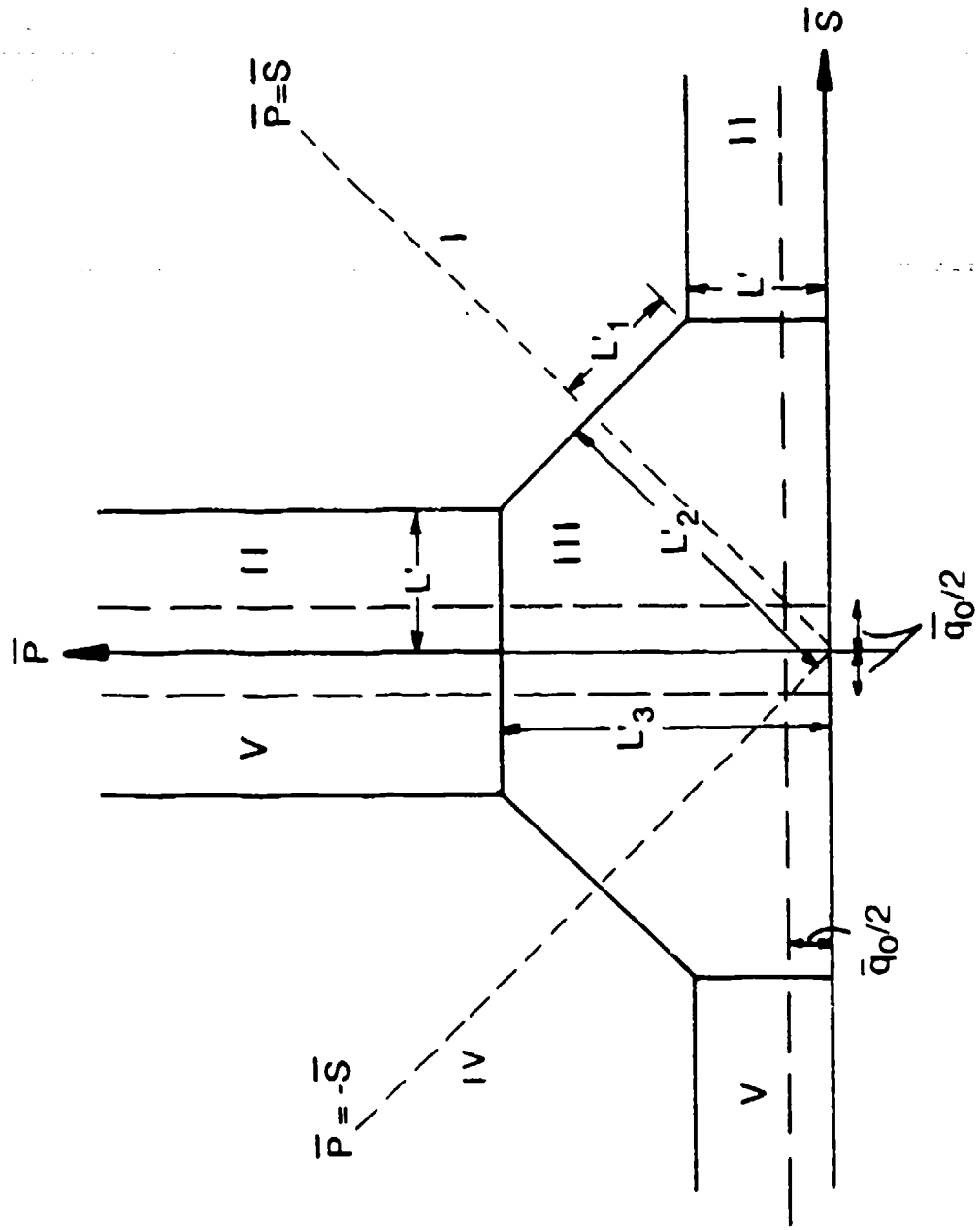

Figure 7. Five regions, I through V in the first and second quadrants of the $\bar{S}$ - $\bar{P}$ plane, are designated for the integrations for the two-position coherence function. Regions II and V individually include two separate areas.

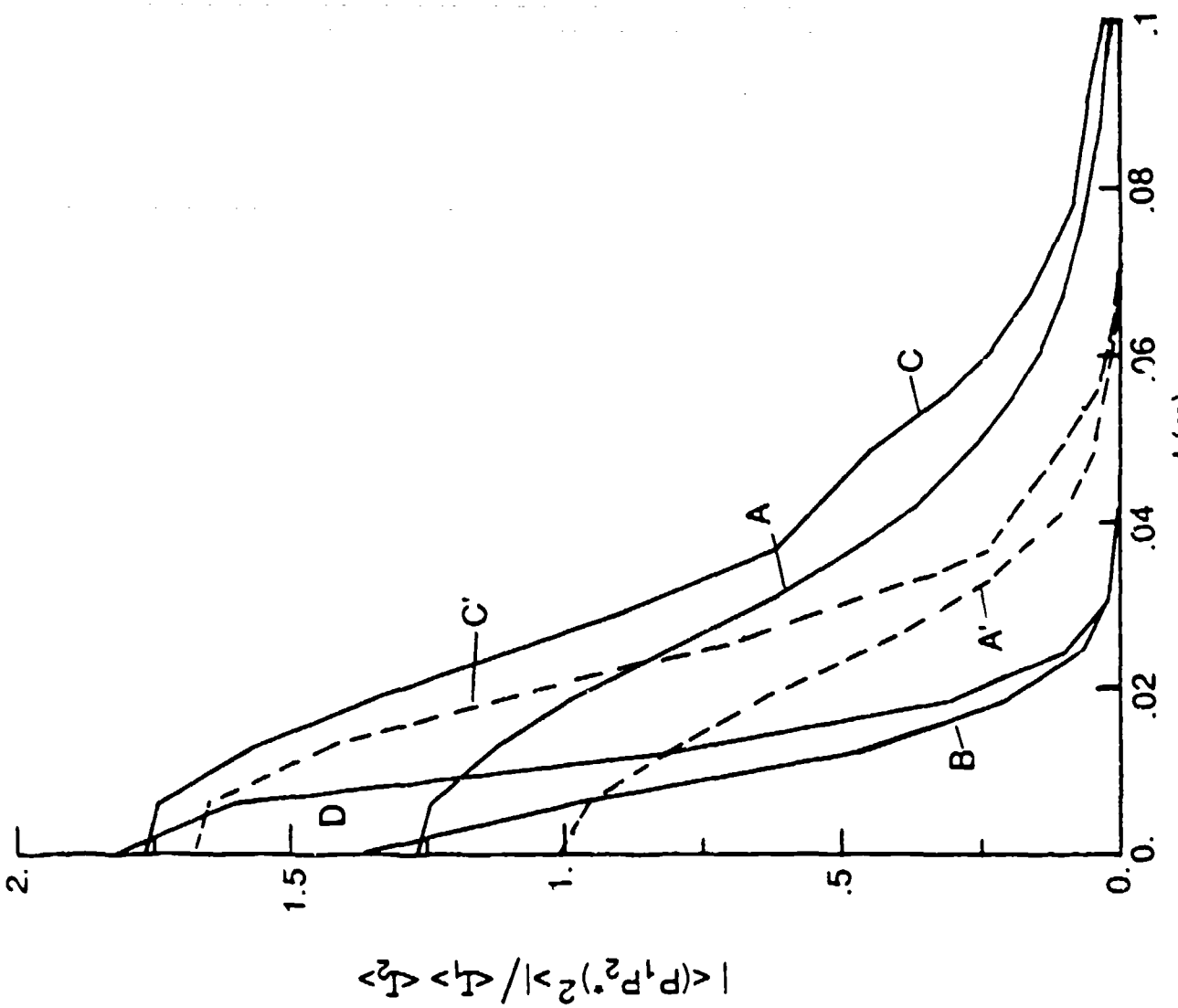

Figure 8. Absolute value of the normalized two-position coherence function versus the separation d. The same letters as those in Figure 6 designate different situations.

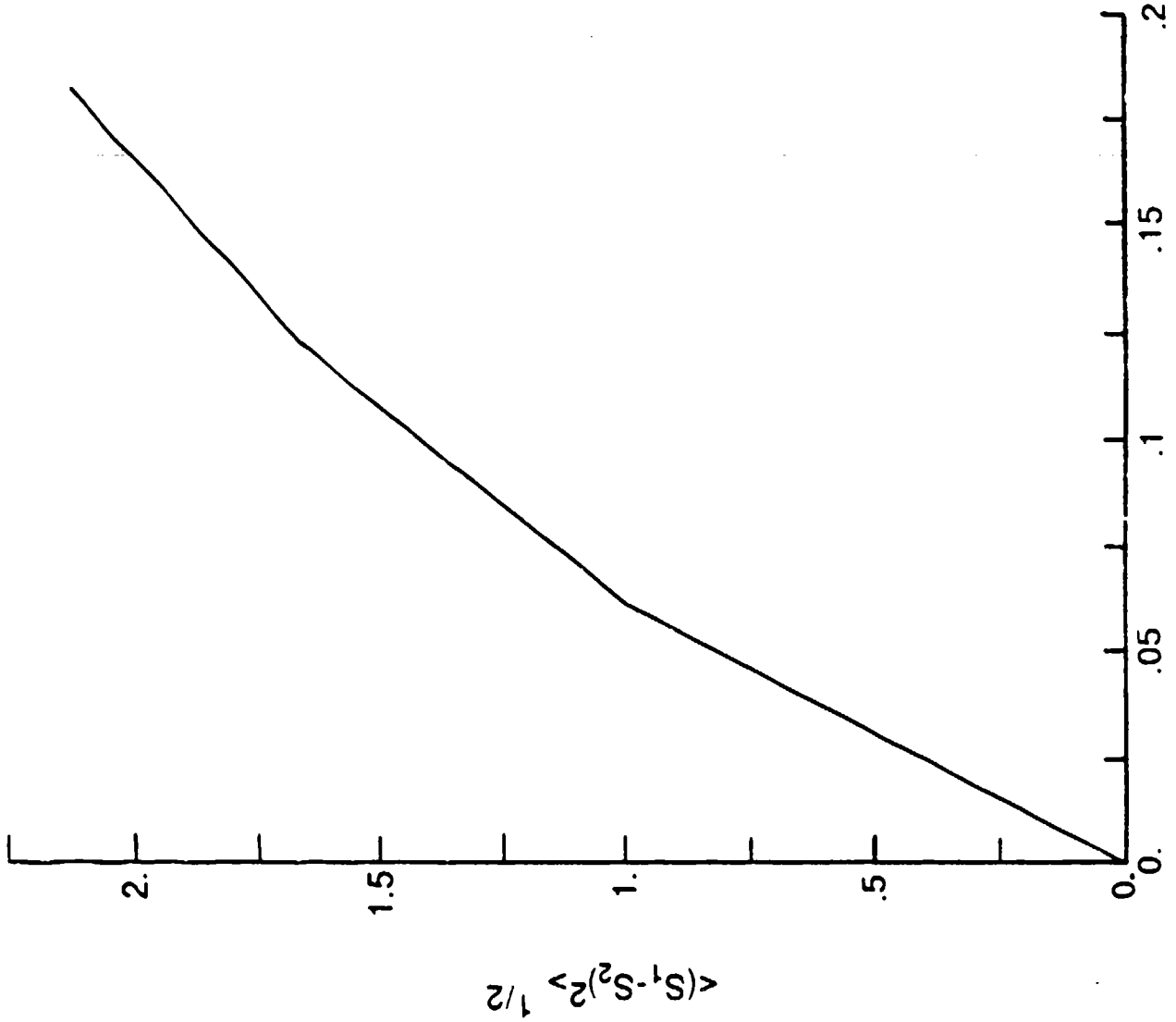

Figure 9. Root-mean-square of the fluctuation of the relative phase between two receivers in the case R = 1 km for a wind speed of 10 m/s and the D/P spectrum.

Distribution List for Unclassified ARL Penn State TM 90-227, entitled, " Fourth Moments of Acoustic Waves Forward Scattered by a Rough Ocean Surface," by C. C. Yang and S. T. McDaniel, dated 9 August 1990.

Office of Naval Research
800 North Quincy Street
Arlington, VA 22217

Attn: M. H. Orr - Code 11250A
Copy No. 1

Naval Coastal Systems Center
Department of the Navy
Panama City, FL 23407-5000

Attn: Gary Sammelmann - Code 2120
Copy No. 2

Naval Oceanographic and Atmospheric
Research Laboratory
Stennis Space Center, MS 39529-5004

Attn: R. W. Farwell - Code 240
Copy No. 3

S. J. Stanic - Code 243
Copy No. 4

Applied Physics Laboratory
University of Washington
1013 N. E. 40th Street
Seattle, WA 98105

Attn: E. I. Thorsos
Copy No. 5

D. R. Jackson
Copy No. 6

Applied Research Laboratory
The Pennsylvania State University
P. O. Box 30
State College, PA 16804

Attn: ARL Library
Copy No. 7